

新型半导体薄膜材料 的制备与光电特性

陈光华 著

兰州大学出版社

图书在版编目 (CIP) 数据

新型半导体薄膜材料的制备与光电特性/陈光华著.
—兰州:兰州大学出版社,2004.4
ISBN 7-311-02373-4

I.新... II.陈... III.①非晶态半导体-研究-文集②电子材料-薄膜-研究-文集
IV.TN304.8-53②TN104-53

中国版本图书馆 CIP 数据核字 (2004) 第 029976 号

新型半导体薄膜材料 的制备与光电特性

陈光华 著

兰州大学出版社出版发行
兰州市天水路 308 号 电话:8617156 邮编:730000
E-mail:press@onbook.com.cn
<http://www.onbook.com.cn>

印刷:甘肃天河印刷有限责任公司
开本:787×1097mm 1/16 印张:24.25

2004 年 4 月第 1 版 2004 年 4 月第 1 次印刷
插页: 字数:584 千字 印数:1-1000 册

ISBN 7-311-02373-4 定价:48.00 元

前 言

薄膜材料由于具有独特且优异的性能,已成为新材料研究和发展的一个重要领域。它在高温、大功率半导体器件、光电信息、电子发射与显示、太阳能利用、材料表面改性、先进涂层技术、航空航天工程等方面有着广泛应用。近年来已受到各国政府的高度重视,将会迅速发展成为一门高新技术产业,并获得巨大的经济效益和社会效益。

我们研究小组(包括我的学生)从 1977 年至今的 25 年中,承担了国家科委六五、七五、八五和九七三攻关任务、国家自然科学基金重大项目 and 多项面上项目、国家教委博士点基金及多项地方政府项目。对各种新型功能薄膜材料的制备、微观结构和特性进行了系统研究和理论分析。特别对非晶硅基合金膜(包括 $a\text{-SiC:H}$ 、 $a\text{-SiGe:H}$ 、 $a\text{-GeN:H}$)、超硬宽隙薄膜(包括:金刚石与类金刚石薄膜、立方氮化硼薄膜、 $\beta\text{-C}_3\text{N}_4$ 薄膜)、富勒烯薄膜(C_{60} 和 C_{70})等材料方面进行了深入研究,取得了多项有创造性的研究成果。在国内外核心刊物上已发表科学论文 400 余篇,11 次获省部级以上科技进步奖。不少研究工作处于当时的国际先进水平,并受到国内外同行专家的高度评价。这里仅将其中有代表性研究成果分为 12 个方面收入本书。

这本论文选集的出版,总结了我们小组 25 年来对非晶半导体和薄膜物理方面的研究内容和方法,同时也反映出我们对这个领域的认识过程和研究思路,以及取得的成果。通过这样的总结,也使我们看到自己的不足,找出差距,从而使我们的研究工作更加深入和更有特色。尤其是,对薄膜材料的物理和化学本质的分析和探索,将会使我们的认识能力得到进一步提高。

在这里要特别感谢和悼念已故的张仿清教授,她在这个小组做了大量的实验和管理工作。她严谨求实的治学态度和对科学及事业忘我的献身精神,以及她的高尚品德,值得我们学习和怀念。

另外,我们在这个领域已出版了《非晶态半导体物理学》(高等教育出版社,1989)、《新型电子薄膜材料》(化工出版社,2002)、《纳米薄膜技术及应用》(化工出版社,2004)和即将出版的《纳米金刚石薄膜制备及应用》(化工出版社,2004)等专著。

目 录

第一部分 非晶半导体理论研究	(1)
1-1* 非晶固体形成能力的理论推导	(3)
1-2* $a-Si_{1-x}N_x:H$ 薄膜拉曼谱的理论研究	(9)
1-3 非晶半导体中杂质和缺陷态的电子统计理论	(15)
1-4 用模拟退火模型研究非晶硅的结构和振动性质	(21)
1-5* 掺硼 $a-SiC:H$ 膜中热诱导缺陷的产生过程	(26)
1-6 非晶 Si 和非晶 Si 基金半导体的 g 因子计算	(34)
1-7 薄膜生长的理论模型与 Monte Carlo 模拟	(39)
1-8* 势阱中杂质薄层对双垒结构共振隧道的影响	(44)
第二部分 非晶硅基合金薄膜的制备及特性研究	(50)
2-1* SiH_4 和 C_2H_4 辉光放电法制备 $a-Si_xC_{1-x}:H$ 膜的光—电特性	(51)
2-2* GD $a-Si_xC_{1-x}:H$ 膜中光电导的吸附和光诱导效应	(59)
2-3* $a-Si_xC_{1-x}:H$ 膜的吸附和表面态研究	(67)
2-4* $a-Si:H/a-Si_xC_{1-x}:H$ 多层膜的瞬态光电导	(73)
2-5* 未掺杂 $a-Si:H/a-Si_xC_{1-x}:H$ 多层膜的瞬态光电导	(80)
2-6* GD $a-Si:H/a-Si_xC_{1-x}:H$ 超晶格的光学性质	(83)
2-7* 用逐次退火法研究 $a-Si:H/a-Ge:H$ 多层膜的结构变化	(86)
2-8 $a-GeN_x$ 和 $a-GeN_x:H$ 薄膜的制备及光电特性的研究	(90)
2-9* 高温退火 $a-SiC:H$ 膜光吸收边的影响	(95)
第三部分 非晶半导体薄膜缺陷态的研究	(102)
3-1* 掺杂 $a-Si_{1-x}C_x:H$ 和 $a-Si_{1-x}N_x:H$ 膜的 ESR 和 IR 研究	(103)
3-2* 由反应溅射法制备的 B-掺杂 $a-Si:H$ 膜的 ESR 研究	(111)
3-3* P, B-掺杂的 $a-Si_{1-x}C_x:H$ 膜的高温 ESR 特性	(117)
3-4* $a-Si_{1-x}C_x:H$ 膜的 LESR 研究	(121)
3-5 氢化非晶锗碳薄膜中的自旋缺陷态	(127)
3-6* 用核反应分析法测量掺杂 $a-SiC:H$ 膜中的氢和硼浓度	(133)
第四部分 非晶硅碳薄膜材料的电子能谱	(137)
4-1 用 XPS 研究 GD- $a-Si_xC_{1-x}$ 膜中等离子体激元的特征	(138)
4-2* RS- $a-Si_xC_{1-x}:H$ 合金膜的 EELS 研究	(143)
4-3* 用电子能量损失谱研究 GD- $a-C:H$ 膜的价电子特性	(146)
4-4* 用 UPS 和 EELS 技术研究 $a-Si_{1-x}C_x:H$ 膜的价电子特性	(149)

4-5*	用 EELS 和 UPS 研究 $a\text{-C:H}$ 膜的价电子行为	(153)
4-6	用紫外光电子能谱研究 $a\text{-Si}_{1-x}\text{C}_x\text{H}$ 的价带特性	(157)
第五部分 窄带隙材料和 $a\text{-Si:H/a-SiGe:H}$ 叠层太阳电池的研究		
5-1*	RF-辉光放电法制备高光敏性 $a\text{-SiGe:H}$ 膜	(163)
5-2*	射频溅射法制备 $a\text{-Si}_{1-x}\text{Sn}_x\text{H}$ 膜的结构特性	(169)
5-3*	衬底温度对溅射 $a\text{-Si}_{1-x}\text{Sn}_x\text{H}$ 合金膜结构的影响	(177)
5-4*	反应溅射法制备的 $a\text{-GeN}_x\text{H}$ 膜的 IR 和 Raman 谱	(181)
5-5*	反应溅射法制备的 $a\text{-GeN}_x\text{H}$ 膜退火行为的 ESR 研究	(185)
5-6	$a\text{-SiGe}_x$ 合金光学常数的研究	(188)
5-7*	用核共振反应分析法研究 $a\text{-Ge:H}$ 膜中氢浓度和分布	(194)
第六部分 非晶半导体膜的电致发光、纳米可见发光及场电子发射的研究		
6-1*	$a\text{-Si}_{1-x}\text{C}_x\text{H/nin-p}$ 结构的注入电致发光	(198)
6-2*	各种结构的 $a\text{-Si}_{1-x}\text{C}_x\text{H}$ 和 $a\text{-Si:H}$ 器件的电致发光	(201)
6-3*	ITO/a-Si:H 结构的注入电致发光	(205)
6-4*	$a\text{-C:H}$ 膜的电致发光研究	(208)
6-5*	$a\text{-C:H}$ 多层膜的电致发光	(212)
6-6*	$a\text{-Si}_{1-x}\text{C}_x\text{H/pn}^-$ 结构的蓝—白电致发光	(216)
6-7	宽带隙薄膜材料场电子发射研究的背景、现状和问题	(220)
6-8	新型金刚石薄膜场电子发射的特性	(226)
第七部分 金刚石和类金刚石薄膜生长机理的研究		
7-1*	CVD-金刚石膜的表面能和形态	(232)
7-2*	用原位光发射谱(OES)研究弧光放电法制备金刚石膜	(238)
7-3*	直流弧光放电法合成金刚石膜的 I-V 特性	(243)
7-4*	氢对金刚石膜和 Zr, Hf 衬底间过渡层的影响	(248)
7-5*	在 Si 和 W 衬底上沉积金刚石膜的生长特性	(254)
7-6*	用 X-射线衍射谱研究金刚石薄膜结构	(262)
7-7	直流弧光放电 CVD 法制备金刚石薄膜及其等离子体的光发射谱原位测量	(268)
7-8*	退火对 $a\text{-C:H}$ 膜光学性质的影响	(273)
7-9	用微波等离子体化学气相沉积(MWCVD)法在(100)Si 衬底上沉积织构金刚石膜	(278)
7-10	织构金刚薄膜的成核与生长	(279)
第八部分 高质量织构立方氮化硼($c\text{-BN}$)薄膜的制备及织构特性研究		
8-1*	在 Ni 衬底上沉积高质量 $c\text{-BN}$ 膜	(286)
8-2*	在 Ni 衬底上 $c\text{-BN}$ 的织构生长	(291)

8-3*	c-BN 薄膜的光学吸收边特性	(295)
8-4	立方氮化硼薄膜的织构生长	(301)
8-5	衬底材料对制备立方氮化硼薄膜的影响	(304)
第九部分 全碳分子(C_{60}, C_{70}···)的合成和特性研究		(310)
9-1*	C_{60} /PMMA 薄膜中 C_{60} 的晶化和取向	(311)
9-2*	C_{60} 薄膜的红外研究	(316)
9-3*	氮掺杂的富勒烯的 ESR 特性	(321)
9-4	氮掺杂富勒烯薄膜电学性质的研究	(329)
9-5	硫掺杂 C_{60} 薄膜电学性质研究	(332)
第十部分 高质量氮化碳($\beta-C_3N_4$)薄膜的制备及特性研究		(336)
10-1	$\beta-C_3N_4$ 的制备及若干问题探讨	(337)
10-2	氮化碳薄膜的结构与特性	(340)
10-3	结晶 $\beta-C_3N_4$ 薄膜的制备和特性研究	(344)
第十一部分 硫系非晶半导体薄膜的制备与特性		(349)
11-1*	Ge 对非晶硫系半导体低温跳跃电导率的影响	(350)
11-2	非晶态 $As_{40}S_{60-x}Se_x$ 薄膜光黑化效应的研究	(356)
11-3	非晶态硫系化合物半导体的制备和电导特性的研究	(361)
第十二部分 微重力和超重力对 InSb 晶体生长的影响		(364)
12-1*	微重力和超重力环境下生长的 InSb 晶体的电学特性	(365)
12-2	微重力环境下 InSb 晶体生长	(370)
附注:未列入本书的最新科研动态		
注:带*的题目为英文		

第一部分 非晶半导体理论研究

非晶态半导体是一门发展极为迅速的新兴学科,是凝聚态物理学中最为活跃的领域之一,已成为材料学科的一个组成部分。大量的事实说明,研究非晶态半导体的意义不仅在技术上能够产生新材料和新器件,而且对于认识固体理论中的许多基本问题也会产生深远的影响。

晶态半导体的基本特征是:组成它的原子或分子作周期性排列,叫作长程有序性。基于这样的特征,利用能带理论,使得晶态半导体中的许多物理问题和半导体器件的基本原理得到了比较满意的解决。而非晶态半导体,在结构上是一种共价无规网络,没有周期性排列的约束,所以它在结构上、光学和电学性质上很不同于晶态半导体。因此,在应用上也显示了自己的特征,已呈现出巨大的应用前景。

同晶态半导体相比,非晶态半导体有以下几个重要的特点:

1. 在结构上,非晶态半导体的组成原子没有长程有序性。但由于原子间的键合力十分类似于晶体,通常保持着几个晶格常数范围内的短程序。简单地说,非晶态半导体结构上是长程无序、短程有序。

2. 对于大多数非晶态半导体,其组成原子都是由共价键结合在一起的,形成一种连续的共价键无规网络,所有的价电子都束缚在键内而满足最大成键数目的 $(8-N)$ 规则,称此为键的饱和性, N 是原子的价电子数。

3. 非晶态半导体可以部分实现连续的物性控制。当连续改变组成非晶态半导体的化学组分时,其比重、相变温度、电导率、禁带宽度等随之连续变化。这样为探索新材料提供了广阔的天地。

4. 非晶态半导体在热力学上处于亚稳状态,在一定条件下可以转变为晶态。这是因为非晶态半导体比其相应的晶态材料有更高的晶格位能,因此处于亚稳状态。

5. 非晶态半导体的结构、电学、光学性质灵敏的依赖于制备条件和制备方法,因此它的性能重复性较差。

6. 非晶态半导体的物理性质是各向同性的,这是因为它的结构是一种共价键无规网络结构。

7. 非晶态半导体材料的制备方法比较简单,大多数材料可以制成薄膜,因此用非晶材料制备的器件成本低廉,容易实现大面积和高容量。

随着非晶态半导体理论的飞速发展,它已在技术领域中得到广泛应用,将形成新的产业。例如:用高效、大面积非晶硅($a-Si:H$)太阳能电池组装的发电站已并网发电;用 $a-Si:H$ 薄膜场效应管作成大屏幕液晶显示器和平面显像电视机已在日本成为商品出售;非晶硫系化合物复印鼓、 $a-Si:H$ 传感器和摄像管、非晶电致发光器件等也正向实际应用和商品化发展。

本部分主要选取了我们研究小组多年来在非晶半导体方面的部分理论研究成果,还有不少工作是结合实验结果提出的理论模型,将这类论文放在相关部分中予以介绍。

①《A Kinetic Treatment of Glass Forming Ability of Solids》一文,是由国际非晶半导体会议常设主席 H. Fritzsche 教授亲自修改原文的,已收入由他主编的《Topics in Non - Crystalline Semiconductors》一书的首篇(1988 年)。该文系统而全面地研究了固体玻璃(非晶态)形成能力,提出了关于“非晶态形成能力”的新判据,纠正了前人出现的错误,发展了非晶形成能力的动力学理论。

②应用量子化学和统计理论,对非晶态半导体结构模型和物性之间的内在联系进行了分析计算,得到了结构缺陷与组分的关系。

③提出了 DBHHN 模型,计算了氢对非晶硅结构的影响。

④最近又提出了热浴模型,用计算机模拟建立了更加接近实际非晶 Si(Ge, C) 系列的结构模型。

1 - 1 A Kinetic Treatment of Glass Forming Ability of Solids

ABSTRACT

In this paper, we calculate the maximum nucleation rate I_m , the maximum crystal growth rate U_m and the critical cooling rate in some materials and discuss the glass forming ability of various amorphous solids.

1. INTRODUCTION

Recently, much progress has been made in both the basic theory and technology of amorphous solids which have become an important new branch of material science.

The theory of glass forming is one of the important subjects in the field of amorphous solids, It is of great significance for the understanding of complex phase - transformations and for the fabrication of new and high quality amorphous materials. A number of authors have discussed the formation of solids. Z. Zheng gave review on this subjects^[1]. Many people were studying the glass forming ability by means of crystallization kinetics. For example, Uhlmann^[2], Davies^[3] and Clavaguena^[4] have calculated the critical cooling rate by means of drawing transformation - temperature - time diagrams for several materials, starting from crystallization kinetics. Vreeswijk et al^[5] have studied this subject from the point of view of nucleation kinetics with the consideration of transient effects. Uhlmann^[6] also discussed the influence of the non - uniform nucleation of the formation of amorphous solids. Although the results deduced by Uhlmann, Davies and Clavaguera from drawing T - T - T diagrams agree fairly well with the experiments results, this is an arduous procedure. The work of Vreeswijk et al.^[5] be facilitated with the help of the computer, these authors have not considered the factor that the different materials have different growth rates. Therefore the critical cooling rate is at variance with the experimental results in their calculations for some materials.

This paper first gives a calculation of the temperature of the maximum value of the nucleation rate and growth rate, and then of the maximum nucleation and growth rate. Finally, the critical cooling rate is calculated by using an analytical formula instead of drawing T - T - T diagrams. Thus the method of finding the critical cooling rate is simplified. It is found that the result agree well with the real case.

2. CRYSTALLIZATION DYNAMICS

According to the crystallization theory developed by Turnbull and Uhlmann, assuming uniform nucleation in the overcooled melt, the nucleation rate I can be expressed as^[4]

$$I = \frac{N_0^0 K T}{3 \pi a_0^3 \eta} \exp \left[- \frac{16 \pi \sigma^3 T_m^4}{3 \Delta H_m^2 R T^3 (T_m - T)^2} \right] \quad (1)$$

Where, N_V^0 is number of molecules per unit volume, k is the Boltzmann constant, a_0 is the molecular diameter, η the coefficient of viscosity, σ the surface interface enthalpy between nucleus and liquid, ΔH_m the enthalpy of melting, R the gas constant. T_m the melting temperature, T the temperature of the liquid.

The growth rate of crystallization U can be expressed by^[4]

$$U = \frac{fkT}{3\pi a_0^3 \eta} \left[1 - \exp\left(-\frac{\Delta H_m (T_m - T)}{RT_m T}\right) \right] \quad (2)$$

In this formula, f represents the fraction of sites on the interface where atoms may preferentially be added or removed. The interface is rough for materials with little melting enthalpy ($\Delta H_m < 2RT_m$), $f = 1$, and the interface is smooth for materials with large melting enthalpy^[2], $f = 0.2(T_m - T/T_m)$.

The viscosity has a strong dependence on temperature, generally described by the Fulcher equation^[5]

$$\eta = A \exp[B/R(T - T_0)] \quad (3)$$

where A is a pre-exponent constant, B is a parameter connected with activation energy, T_0 is the transformation temperature of the ideal glass.

For σ , we use an empirical relation

$$\sigma = a\Delta H_m \quad (4)$$

where $a = 0.32$, so

$$\sigma = 0.32\Delta H_m \quad (4')$$

We substitute Eq (3) and (4') into (1) and (2), and let

$$\alpha = k/3aA, \beta = \frac{B}{R}, \theta = \frac{\Delta H_m}{RT_m}, \text{ and}$$

$$\gamma = \frac{16\pi (0.32)^2 \Delta H_m T_m^4}{3R}$$

and obtain

$$I = N_V^0 \alpha T \frac{\exp[-\gamma/T^3(T_m - T)^2]}{\exp[\beta/(T - T_0)]} \quad (5)$$

$$U = f a_0 T \frac{[1 - \exp(-\theta(T_m/t - 1))]}{\exp[\beta/(T - T_0)]} \quad (6)$$

To determine the temperature at which I reaches its maximum value, we set $dI/dT = 0$ and obtain

$$1 + \frac{\beta T_1^2}{(T_1 - T_m)^2} - \frac{2\gamma}{T_1^2(T_m - T_1)^3} + \frac{3\gamma}{T_1^3(T_m - T_1)^2} = 0 \quad (7)$$

The values of T_1 obtained from this equation are listed for several materials in Table I.

In the same way, to determine the temperature T_u at which U reaches its maximum value, we set $dU/dT = 0$, and obtain

$$T_u + \frac{\beta T_u^2}{(T_u - T_0)^2} - (T_u + \frac{\beta T_u^2}{T_u - T_0} + \theta T_m) e^{\theta(1 - T_m/T_u)} = 0 \quad (8)$$

The value of T_u obtained from this equation can also be found in Table I.

The values I_m obtained by calculation for the maximum nucleation rate can be found in Table I. Just in the same way, by substituting the value of T_u into Eq. (6), one obtains the values for the

maximum growth rate list in Table I.

Table 1. Calculated data for the temperature and magnitudes of maximum nucleation and crystallization rates for various materials.

	P ₂ O ₅	GeO ₂	As ₂ O ₃	BeF ₂	ZnCl ₂	BiCl ₃	CCl ₄
T _i (k)	540	870	690	760	350	310	150
T _u (k)	820	1310	990	1030	530	440	220
I _m (cm ⁻³ s ⁻¹)	1.4 × 10 ⁻¹⁸	2.2 × 10 ⁻⁸	5.9 × 10 ¹¹	3.6 × 10 ⁻³	5.7 × 10 ⁻¹⁷	1.4 × 10 ⁹	1.6 × 10 ¹¹
U _m (cm ⁻³ s ⁻¹)	4.9 × 10 ⁻⁹	2.5 × 10 ⁻⁶	8.8 × 10 ⁻⁴	4.0 × 10 ⁻⁸	1.2 × 10 ⁻⁷	1.1 × 10 ⁻²	1.1 × 10 ⁻¹
	C ₆ H ₆	NaCl	Na ₂ CO ₃	NaNO ₃	Cu	Sn	Pb
T _i (k)	170	660	700	350	850	310	370
T _u (k)	240	930	1050	490	1100	380	470
I _m (cm ⁻³ s ⁻¹)	2.7 × 10 ⁻²	3.5 × 10 ⁵	3.7 × 10 ⁴	2.2 × 10 ⁶	3.8 × 10 ²²	1.9 × 10 ¹⁸	5.4 × 10 ²²
U _m (cm ⁻³ s ⁻¹)	3.0 × 10 ⁻²	1.4	1.6 × 10 ⁻¹	3.8 × 10 ⁻¹	8.6 × 10 ⁻¹	8.0 × 10 ⁻¹	3.5 × 10 ⁻¹

The criterion for glass formation is obtained by asking how fast the cooling rate need be to avoid obtaining crystallites. Now we consider a material with a definite melting point and neglecting the transient effect. With the time interval t , for small χ value, the relation between percentage of volume crystallization χ and uniform nucleation rate I is

$$\chi \approx \frac{1}{3} \pi I U^3 t^4 \quad (9)$$

Substituting Eqs. (5) and (6) into (9), we obtain

$$t = \left(\frac{3\chi}{\pi N_0^0 a_0^3 f^3} \right)^{1/4} \frac{1}{\alpha T} \frac{e^{\beta/(T-T_0) + r/4T^3(T_m-T)^2}}{[1 - e^{-\theta(T_m/T-1)}]^{3/4}} \quad (10)$$

From Eq. (10), we get the temperature T_N at the minimum value of t . The equation obtained from formula (10) yields

$$4T_N + \frac{4\beta T_N^2}{(T_N - T_0)^2} + \frac{3r}{T_N^2(T_m - T_N)^2} - \frac{2r}{T_N(T_m - T_N)^3} = \frac{3\theta T_m}{[e^{\theta(T_m/T_N-1)} - 1]} \quad (11)$$

Generally we suppose that the percentage of volume crystallization with the value of $X = 10^{-6}$ is clearly measurable, i. e. the detectable concentration of crystallization. We take the value $X = 10^{-6}$ as critical percentage of volume crystallization, i. e. when χ is less than 10^{-6} , an amorphous solid has been formed.

Using Eq. (11), we calculated the critical volume for several materials. The results are listed in Table II. Substituting the value of T_N into Eq. (10), one obtains the values of t_N listed in Table II. So the critical cooling rate Q^* is obtained from

$$Q^* \approx (T_m - T_N)/t_N \quad (12)$$

The results are also listed in Table II.

Table II. Calculated data of T_N , t_N , and Q^* for fourteen materials

	P ₂ O ₅	GeO ₂	As ₂ O ₃	BeF ₂	ZnCl ₂	PbBr ₂
T _N (K)	594	965	753	790	79	408
T _N (s)	2.3×10^{12}	3.9×10^7	6.8×10^{-2}	3.2×10^7	5.8×10^{10}	2.2×10^{-2}
Q* (K/s)	1.1×10^{-10}	1.0×10^{-5}	4.6×10^3	8.7×10^{-6}	2.9×10^{-9}	1.0×10^4
	BiCl ₃	CCl ₄	C ₆ H ₆	NaCl	NaNO ₃	Na ₂ CO ₃
T _N (K)	328	160	176	685	367	767
T _N (s)	1.4×10^{-2}	2.0×10^{-1}	3.6	2.5×10^{-3}	3.9×10^{-3}	0.16
Q* (K/s)	1.3×10^4	4.5×10^2	2.9×10	1.6×10^5	5.5×10^5	2.3×10^3
	Na ₂ SO ₄	Na ₂ WO ₄	Ag	Cu	Sn	Pb
T _N (K)	627	753	812	901	318	393
T _N (s)	1.0×10^{-3}	4.8×10^{-5}	1.3×10^{-8}	1.2×10^{-7}	1.2×10^{-6}	1.7×10^{-7}
Q* (K/s)	3.4×10^5	8.5×10^6	3.3×10	3.9×10^9	1.6×10^8	1.3×10^9

3. DISCUSSION

(1) According as the calculated data listed in Table I. The glass forming ability of fourteen kinds of materials can be arranged as follows in order of $(T_u - T_l)/T_l$ value:

ZnCl₂ → P₂O₅ → GeO₂ → Na₂CO₃ → As₂O₃ → CCl₄ → C₆H₆ → NaCl → BiCl₃ → NaNO₃ → Cu → Pb → Sn. To compare with these relatively too low (Sn, C₆H₆ and CCl₄) or too high (As₂O₃) values as calculated by Vreeswijk et al⁵ our calculated data better agree with the experimental results. It can be concluded that $(T_u - T_l)/T_l$ is one of the criteria for the glass forming ability of materials⁷.

(2) In this method, we have calculated the critical cooling rate for some materials for forming amorphous solids. On the whole, the results agree with the experiment results. From the value of Q*, it can be seen that the cooling rate necessary for the formation of amorphous solids very widely among various materials (e.g. in our calculation, the variation is of the order of 10²⁰). Therefore, some materials can form amorphous solids under the condition of free cooling, but some materials have not been transformed into amorphous solids with the present techniques.

(3) Generally speaking, some materials are good glass formers, because not only their nucleation rate is low, but also their growth rate is comparatively low, and its maximum nucleation rate has a great variation with its growth rate, i.e. their overlap is small. This is the reason why some materials are hard to be transformed into crystals in nature. Even if they have nucleated, there is no condition for growth. On the other hand, if the growing condition is offered, the nuclei are missing.

In contrast, some materials are good crystallization formers, not only because their nucleation rate is high, but also their growth rate is comparatively large, and maximum nucleation rate is close to the maximum value of the growth rate, i.e. their overlap is large. This also accounts for the reason why some materials are hard to be formed into amorphous solids. That is, once they have nucleated, proper condition is provided for their growth, and their nucleation rate is high, the growth rate is also large.

All these situations can be summarized in Fig. 1, 2, and 3. In addition, we have calculated the

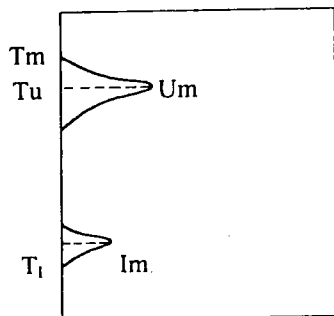


Fig. 1. Amorphous solids with good Glass-forming ability

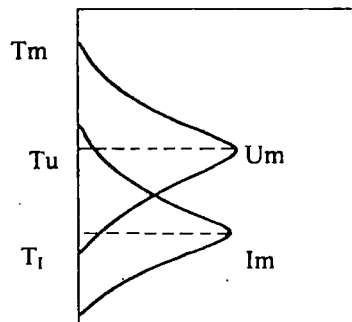


Fig. 2. Normal amorphous solids

growth rate at the maximum nucleation rate and the nucleation at the maximum growth rate for Cu and GeO_2 . For example, the nucleation rate at the maximum growth rate is $5 \times 10^{16} \text{ cm}^{-3} \text{ s}^{-1}$ for Cu, but the value tends to be zero for GeO_2 .

(4) For different materials, the maximum nucleation rates differ greatly. Among the materials we have calculated, for example, the maximum nucleation rate for P_2O_5 is $1.4 \times 10^{-18} \text{ cm}^{-3} \text{ s}^{-1}$, while for Cu $3.8 \times 10^{22} \text{ cm}^{-3} \text{ s}^{-1}$. The variance of the maximum nucleation rate for the two materials is of the order 10^{40} . However, the variance of the maximum growth rate for various materials such as P_2O_5 ($U_m = 4.9 \times 10^{-9} \text{ cm/s}$) and Cu ($U_m = 8.6 \times 10^{-1} \text{ cm/s}$) is of the order 10^8 .

(5) The value of η has a considerable influence on the nucleation rate, growth rate, and the critical cooling rate (In our calculation, the changing range is of the order 10^{12}), i.e. B affects them remarkably. It is easier for the materials with larger B value to form amorphous solids while other data have small differences. The ΔH_m value affects the nucleation rate and the cooling rate considerably, but not the growth rate. It is easier for the materials with higher ΔH_m value to form amorphous solids while other data have small differences.

On the other hand, it is easier for the materials with higher T_m value to form amorphous solids than with lower T_m value. This result indicates that when metals are formed into alloys and the point of co-crystallization is lower than the melting point of the original metals, the cooling rate decreases. So it is easier to form amorphous solids.

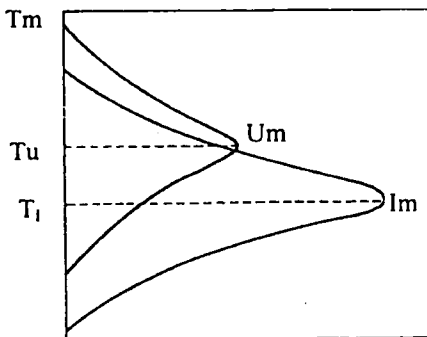


Fig. 3. Good crystallization solids

REFERENCES

- [1] Zheng Zhaobo, Acta Metallurgical Sinica (Chinese) 15, 155 (1979).
- [2] Uhlmann, D.R., J. Non-cryst. Solids 7, 337 (1972).
- [3] Davies, H.A., J. Non-cryst. Solids 17, 266 (1975).

- [4] Clavaaguera, N., Clavaguera - Mora, M.T. and Casasvazquez, J., Non - cryst. Solids 22, 23 (1976).
- [5] Vreeswijk, J.C.A., Gossink, R.G. and Stevels, J.M.J. Non - cryst. Solids 16, 15 (1974).
- [6] Onorato, P.I.K. and Uhlmann, D.R., J. Non - cryst. Solids 22, 367 (1976).
- [7] Wu Jinhua, Zhang Fangqing, and Chen Guanghua, Phys. stat. Sol. (a)101, K1 (1987).

1 - 2 Theoretical Study of the Raman Spectrum in a - Si_{1-x}N_x:H Films

The vibrational excitations in a - Si_{1-x}N_x:H films are calculated in terms of a simplified amorphous cluster. The main vibrational modes as well as correlative frequencies and intensities are obtained. By means of a random substitution of nitrogen atoms for silicon atoms the phonon density of states at different x values are deduced. It can be found that the results are in accord with the experimental Raman spectra.

Die Schwingungsanregungen in a - Si_{1-x}N_x: H - Schichten werden mit einem vereinfachten amorphen Cluster berechnet. Sowohl die mittleren Schwingungsmoden als auch die Korrelationsfrequenzen und - Intensitäten werden erhalten. Mittels statistischer Substitution von Stickstoffatomen für Siliziumatome wird die Phononenzustandsdichte bei verschiedenen x - Werten abgeleitet. Es wird gefunden, daß die Ergebnisse in Übereinstimmung mit experimentellen Ramanspektren sind.

1. Introduction

The Raman scattering technique has been used to investigate the structural disorder in amorphous Si - based alloys and revealed to be a useful tool [1]. In order to help analysing experimental Raman spectra, it is necessary to clarify the main vibrational modes in amorphous silicon materials theoretically. Furthermore, it is desirable to know how the corresponding modes change, as the microstructure of the materials changes. Thus some useful information for analysing Raman spectra can be provided. Therefore, in this paper several typical clusters are constructed for a - Si_{1-x}N_x:H films and their vibrational modes are calculated. By means of a statistical average method on the basis of a random distribution, the phonon density of states (PDOS) is obtained and the results are compared with experiments.

2. Calculation Method

After some of the clusters were calculated, we paid attention to two kinds of simplified clusters shown in Fig. 1. Since the hydrogen atom has small effect on Raman shift, there is no hydrogen atom in our cluster. We assumed that there is no nitrogen-nitrogen bond, as the content of nitrogen is not high. For the two clusters, when the local vibrational modes of its central atom are investigated, effects of the atoms not only at nearest neighbour sites but also at next neighbour sites, are considered. Although we discuss a simplified cluster, the essential vibrational modes in the sample are involved.

We used a valence force field model with the Keating potential[2], that comes from [3], and obtained a force constant matrix

$$\Phi_{ij}^{\alpha\beta} = \left(\frac{\partial^2 V(KP)}{\partial u_i^\alpha \partial u_j^\beta} \right)_{u=0}$$

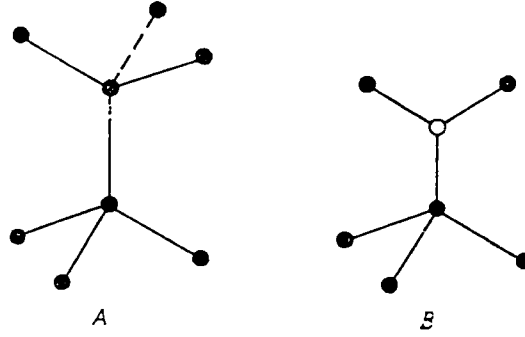


Fig.1. The two clusters discussed by us. The solid circle represents a silicon atom and open circle represents a nitrogen atom

Where $V(KP)$ is the Keating potential, u_I^α the α -th component of the displacement vector of the I -th atom. Then the eigen equation is

$$\sum_{j=1}^N \sum_{\beta=1}^3 \phi_{Ij}^{\alpha\beta} e_j^\beta = m_I \omega^2 e_I^\alpha$$

where m_I is the mass of the I -th atom, e_I^α the α -th component of the eigen vector of the I -th atom. Through numerical calculation the eigen frequencies and the eigenvectors were obtained, while each eigen vector was fitted to the normalizing condition

$$\sum_{I=1}^N \sum_{\alpha=1}^3 |e_I^\alpha(i)|^2 = 1$$

Because of the existence of random structural relaxation in an amorphous solid, each spectral line obtained from the calculation, in fact, should be a band with certain width. Therefore the local phonon density of states (LPDOS) of the I -th atom may be written as the Gauss distribution,

$$Q_I(\omega) = \sum_i H_i \exp \left[-\frac{(\omega - \omega_i)^2}{\sigma^2} \right],$$

where the weight factor H_i is the intensity of the i -th vibrational mode and it may be obtained from the equation

$$H_i = \sum_{\alpha=1}^3 |e_I^\alpha(i)|^2,$$

where σ is the width of the corresponding spectral line and is estimated to be 10cm^{-1} .

Let the $a\text{-Si}_{1-x}\text{N}_x$ sample consist of M atoms, of which M_1 atoms are silicon and M_2 atoms nitrogen, and $x = M_2/M$. For given x -value, the number of nitrogen atoms distributed into each cluster is not definite. If the occupation of a site by a silicon or nitrogen atom is stochastic, the probability of the occupation of Z sites by nitrogen atoms in the cluster with N atoms can obey a super-geometrical distribution,

$$P_{M, M_2, N}(Z) = \frac{C_{M_2-N}^{M_2-Z} C_N^Z}{C_M^{M_2}},$$

Theoretical Study of the Raman Spectrum in $a\text{-Si}_{1-x}\text{N}_x\text{:H}$ Films

where $C_m^n = m! / n! (m-n)!$. Taking account of M and $M_2 \gg N$ and Z and using Stirling's approximation,

$$\ln m! = m(\ln m - 1),$$

we obtain

$$P_{M, M_2, N}(Z) \equiv P_N(x, Z) = C_{Nt}^Z (1-x)^{N-Z}.$$

Thus the PDOS in an $a\text{-Si}_{1-x}\text{N}_x\text{:H}$ sample can be deduced from LPDOS of various clusters with different Z value, It can be written as

$$Q_x(\omega) = \sum_I \sum_Z P_N(x, Z) Q_I(\omega, Z),$$

where the sum over I is over the central atoms of the cluster – assigned Z value.

3. Result and Discussion

3.1 The vibrational modes

The dominant vibrational modes obtained from our cluster are shown in Fig.2 and some of their properties are shown in Table 1. It can be seen that the vibrational frequencies arising from the Si – N bond are higher than the corresponding vibrational frequencies arising from the Si – Si bond. However, the behaviour of the TA – like vibrational modes is different from that of the TO – like modes. The TA – like modes indicate the collective vibration of a cluster. When a silicon atom is substituted by nitrogen, the total mass of the cluster is slightly diminished, which results in a small increase of the frequencies of TA – like modes. As contrasted with TA – like modes, the TO – like modes indicate the relative vibration among atoms in a cluster. With silicon substituted by nitrogen, the equivalent mass of the cluster and the bond lengths among atoms are changed. Therefore the frequencies of the TO – like modes are so much moved that some new frequencies appear in further sites.

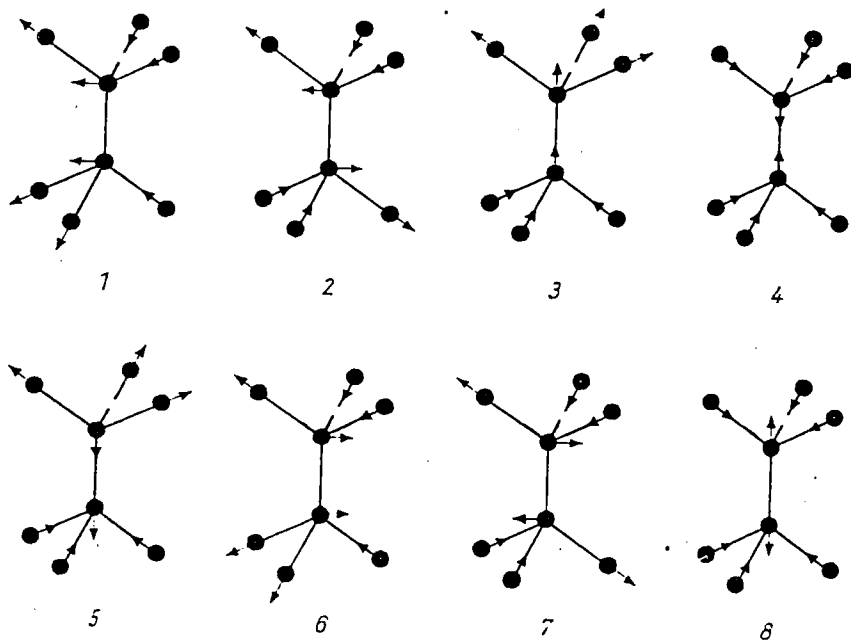


Fig. 2. The main vibrational modes obtained from cluster A